RESEARCH ARTICLE

{M}acro-molecular
Rapid Communications
www.mrc-journal.de

Copper-Coordinated Covalent Organic Framework Produced a Robust Fenton-Like Effect Inducing Immunogenic Cell Death of Tumors

Tong Li, Dianwei Wang, Meng Meng, Zhiyu Yang, Zhimin Luo, Zhen Li, Fei Li, Cong Liu, Kai Hao,* Xuan Pang, Huayu Tian,* and Xuesi Chen

Increasing infiltration of CD8$^+$ T cells can enhance the response rate to immune checkpoint blockade (ICB) therapies. In contrast, immunogenic cell death (ICD) induced by intracellular reactive oxygen species (ROS) is an effective strategy to increase CD8$^+$ T cell infiltration. Cuproptosis is newly defined and reported by Tsvetkov et al. A Cu-coordinated covalent organic framework (COF) in which two valence states of copper ions are simultaneously loaded is prepared. On the one hand, Cu^{2+} undergoes a valence shift generating Cu$^+$ which acts as an effective Fenton-like reagent to catalyze the production of $\cdot$OH and $^1O_2$ from cellular overexpressed H$_2$O$_2$, causing DNA damage and lipid peroxidation (LPO), which directly produce cytotoxicity. On the other hand, residual Cu^{2+} can effectively deplete endogenous cellular glutathione (GSH), converting it into glutathione disulfide (GSSG), further increasing intracellular oxidative stress and reducing the scavenging of ROS, thus further enhancing the Fenton-like effect and bringing toxic effects on tumor cells. The synergy of these two functions achieves ICD, helping for transforming "cold tumor" into "hot tumor" and efficient anti-tumor effects eventually. This work provides new insights into coordinated COF and inspire the development of more versatile COF for biomedical applications.

1. Introduction

The tumor microenvironment (TME) has been reported to have an impact on the effectiveness of immunotherapy in tumors.[1] T-cell infiltration in the TME is critical for the success of immune checkpoint blockade (ICB).[2] Based on the amount of T-cell infiltration within the tumor, tumors are simply classified as "cold tumors" and "hot tumors". "Hot tumors" have a higher response rate to ICB therapy than "cold tumors" because of more CD8$^+$ T cells. Therefore, increasing the response rate to ICB therapy could be achieved by increasing the infiltration of CD8$^+$ T cells.[3]

Immunogenic cell death (ICD)[4] is an effective method of enhancing CD8$^+$ T cell infiltration. It increases the immune response of T cells by releasing tumor-associated antigens and damage-associated molecular patterns (DAMPs),[5] which further trigger effective antigen presentation. One of the important inducers of ICD is intracellular rea tve ROS,[5] which is a key factor in the induction of ICD, reflecting in the cal- reticulin (CRT) exposure, release of high-mobility group box-1 (HMGB1), and adenosine triphosphate (ATP) secretion. Therefore, by achieving intracellular ROS production, it is expected to bring effective tumor inhibition. Chemodynamic therapy based on the Fenton effect was therefore of interest to us. On the other hand, oxidative stress occurs after intracellular ROS production and the presence of antioxidants such as glutathione (GSH)[6] increases to quench ROS. Therefore, the removal of GSH can enhance the killing effect of the Fenton effect.[7]

T. Li, D. Wang, M. Meng, Z. Yang, Z. Li, X. Pang, H. Tian, X. Chen
Key Laboratory of Polymer Ecomaterials
Changchun Institute of Applied Chemistry
Chinese Academy of Sciences
Changchun 130022, China
E-mail: thy@xmu.edu.cn
T. Li, D. Wang, M. Meng, Z. Yang, Z. Li, X. Pang, H. Tian, X. Chen
University of Science and Technology of China
Hefei 230026, China

T. Li, D. Wang, M. Meng, Z. Yang, Z. Li, X. Pang, H. Tian, X. Chen
Jilin Biomedical Polymers Engineering Laboratory
Changchun 130022, China
T. Li, M. Meng, Z. Yang, Z. Luo, Z. Li, F. Li, C. Liu, K. Hao, H. Tian
State Key Laboratory of Physical Chemistry of Solid Surfaces
Xiamen University
Xiamen 361005, China
E-mail: kaihao@xmu.edu.cn
H. Tian
College of Chemistry and Chemical Engineering
Xiamen University
Xiamen 361005, China
H. Tian
Innovation Laboratory for Sciences and Technologies of Energy Materials
of Fujian Province (IKKEM)
Xiamen 361005, China
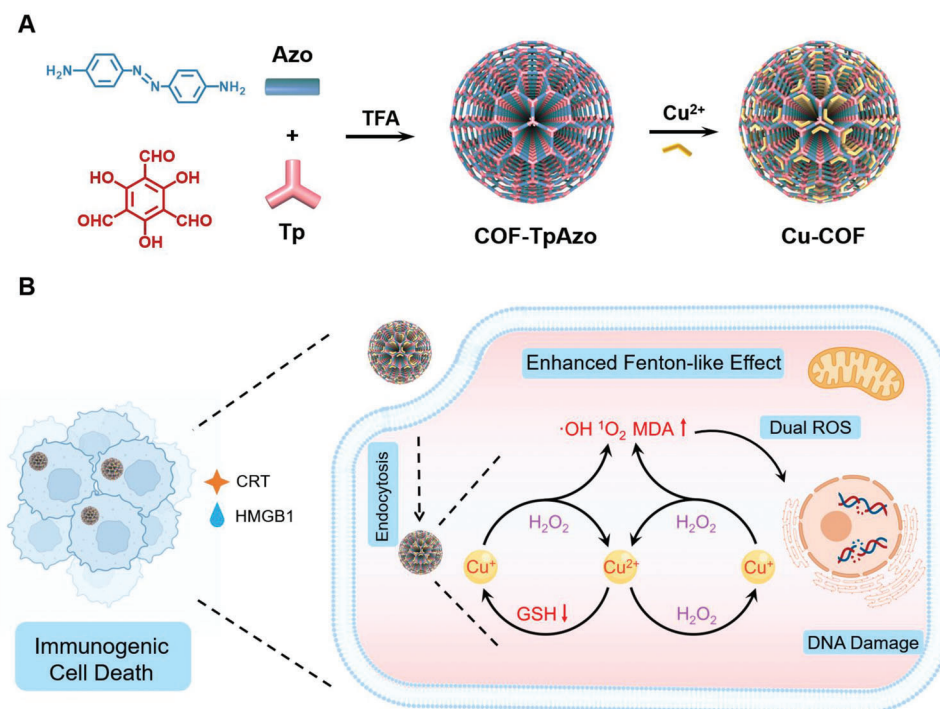
Scheme 1. Schematic illustrations of the formation of Cu-COF and the enhanced Fenton-like effect to induce ICD. A) Preparation method of Cu-COF. B) Schematic diagram of enhanced Fenton-like effect induced by Cu-COF. TFA: trifluoroacetic acid.

Excess iron[8] can trigger ferroptosis through ROS produced by the Fenton effect and activation of iron-containing enzymes (such as lipoxygenases) to promote lipid peroxidation (LPO).[9] There have been many outstanding works on the excellent ability of Cu to induce ICD effect.[10] Copper-based Fenton-like reagents exhibit better catalytic activity compared to Fe^{2+}.[10] Differing from the other known forms of cell death, cuproptosis[11] was recently defined and reported as a copper-dependent non-apoptotic form of cell death by Tsvetkov et al. They found that the mechanism by which excess copper leads to cell death involves the disruption of specific mitochondrial metabolic enzymes and was termed as cuproptosis.[12] However, it is very difficult to obtain Cu^+ directly in solution as it is very easily oxidized to produce Cu^{2+} and loses its catalytic activity. It has been reported that the stable Cu^+ could be present in some Cu-based metal-organic complexes,[13] and it may be that coordination interactions which stabilized the valence state of Cu^+. Covalent organic framework (COF) materials have been emerging in several fields due to their unique properties since found by Yaghi in 2005.[6b] In recent years, they have gained more attention in the biomedical field.[14] Considering the good coordination and biocompatibility of Cu, we expect that the design and synthesis of Cu-coordinated COF could lead to a stronger Fenton-like effect and direct killing of tumor cells.

In this work, we coordinated Cu^{2+} on the COF-TpAzo. After coordination, part of Cu^{2+} had valence conversion and became Cu^+, leading to the simultaneous loaded Cu^{2+} and Cu^+ in Cu-COF (**Scheme 1**A). After entering the cells, Cu^+ catalyzed the decomposition of overexpressed hydrogen peroxide (H_2O_2) in the cells to produce $\cdot OH$ and $^1O_2$. These two highly cytotoxic ROS could cause obvious DNA damage[15] and lipid peroxidation, directly

killing the cell. At the same time, Cu^{2+} consumed GSH to convert it into glutathione disulfide (GSSG), reducing the elimination of ROS, thereby further enhancing the Fenton-like effect and bringing toxicity to cells (Scheme 1B). In this work, copper-coordinated COF was modified to kill tumor cells, inducing robust ICD to transform "cold tumor" into "hot tumor", which made a meaningful exploration and attempt for the application of COF in the biomedical field.

2. Results and Discussion

2.1. Preparation and Characterization of Cu-COF

We first synthesized COF nanoparticles according to the methods reported in the literature.[16] The synthetic route was shown in Figure S1. COF was obtained by stirring two monomers, 4,4'-azodianiline (**Azo**) and 1,3,5-triformylphloroglucinol (**Tp**) in dichloromethane solvent. As a catalyst, trifluoroacetic acid (TFA) was introduced into the reaction system to control the particle size of the prepared COF. Then Cu^{2+} ions were coordinated into COF to prepare Cu-COF. It was obtained by heating reflux using anhydrous $CuSO_4$ and COF in DMF solvent and washing with water to remove the uncoordinated Cu^{2+} ions. It could be observed that the originally bright red COF shifts to purple after coordination. The synthesized COF and Cu-COF were characterized using Fourier transform infrared spectroscopy (FT-IR). As the results in **Figure 1**A shown, the decrease of the characteristic peak of amino group (−N−H) on Azo at 3336 cm^{-1}, the characteristic peak of Tp aldehyde group at 2891 cm^{-1}, and a new absorption band at 1618 cm^{-1} indicated the occurrence of Schiff base reaction. While in Cu-COF the absorption band was shifted
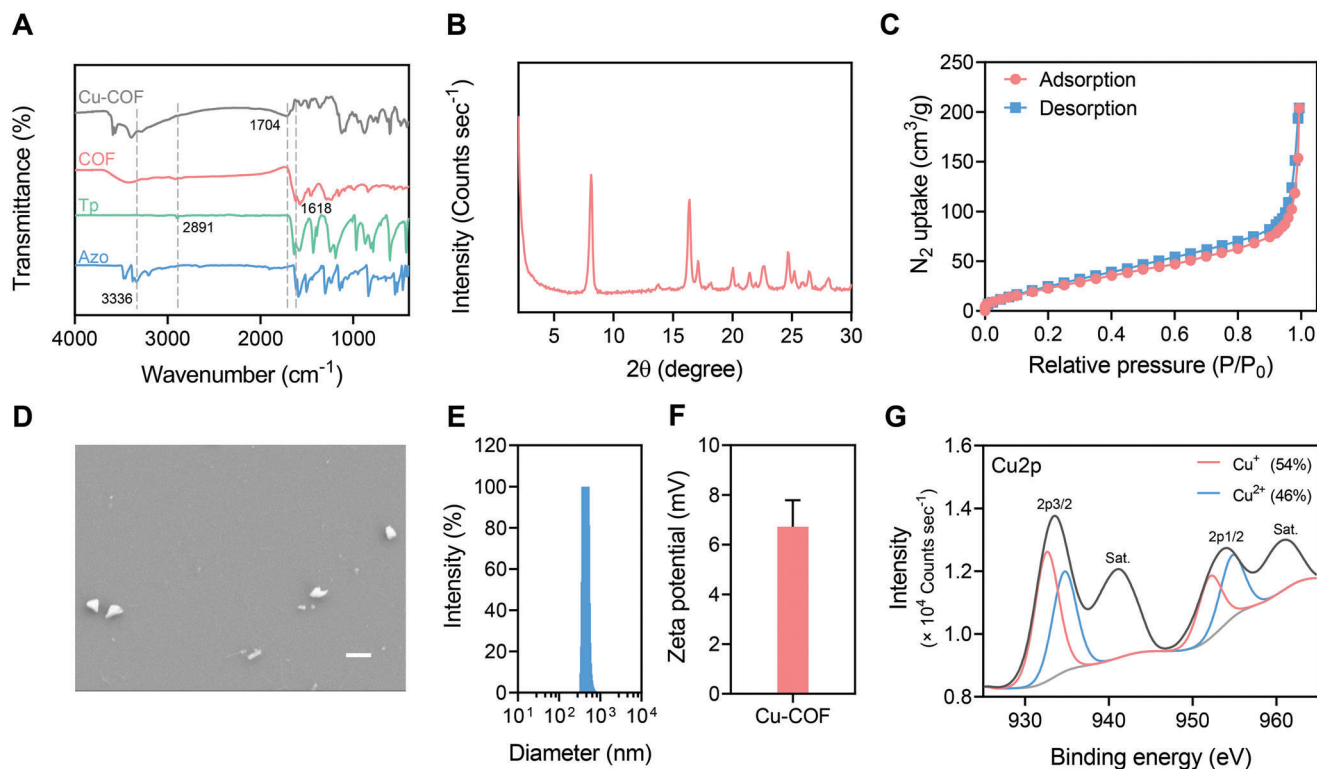
Figure 1. Preparation and characterization of Cu-COF. A) The FT-IR spectra of Tp, Azo, COF, Cu-COF. B) The PXRD spectra of Cu-COF. C) N_2 adsorption-desorption isotherms of Cu-COF at 77 K. D) SEM image of Cu-COF, scale bar = 1 μm. E) DLS result of Cu-COF. F) Zeta potential result of Cu-COF. G) XPS spectra of Cu-COF in Cu2p binding energy region and analyzed by Avantage.

to 1704 cm^{-1} and the change in peak position tentatively indicated the successful coordination of Cu ions.[17] The PXRD results in Figure 1B showed that after Cu coordination, the (100) crystal plane peak of COF at 3° disappeared and changed to a strong peak at 8.1°, which corresponded to the (020) plane, indicating the high crystallinity of Cu-COF. From N_2 adsorption-desorption isotherms at 77 K, Cu-COF had a typical I-type nitrogen absorption-desorption curve with Brunauer–Emmett–Teller (BET) surface area of 95.339 m$^2 \cdot$g^{-1} (Figure 1C). The average pore diameter of Cu-COF was 2.183 nm. (Figure S2, Supporting Information). We then observed the morphology of Cu-COF under a scanning electron microscope (SEM). As shown in Figure 1D, we found Cu-COF in irregularly shaped nanoparticles. Combined with the XRD and nitrogen adsorption results, we speculated that the coordination effect of Cu caused different degrees of damage to the original COF structure, making the obtained Cu-COF not very homogeneous in shape. DLS results in Figure 1E showed that the particle size of Cu-COF was 443.1 ± 41.1 nm, in general agreement with the SEM results, and the zeta potential was ≈6.7 mV (Figure 1F). The weak positive charge was favorable for Cu-COF to be adsorbed by the negative electricity on the cell membrane surface. As shown in Figure 1G, the X-ray photoelectron spectroscopy (XPS) spectrum revealed peaks at 934/954 eV and 932/952 eV, which corresponded to Cu^{2+} and Cu$^+$ respectively. After calculation, it was concluded that there were ≈54% Cu$^+$ and 46% Cu^{2+} within the Cu- COF.

Thermogravimetric analysis (TGA) profiles of COF in Figure S4, Supporting Information, revealed its excellent thermal sta-

bility of more than 400 °C. However, after Cu coordination, the stability of Cu-COF decreased slightly. It is speculated that the intercalated copper has some influence on the structure of COF.

2.2. Functional Characterization of Cu-COF

After successfully synthesizing Cu-COF, we further explored its functions in detail. Time-dependent release of copper from Cu-COF under different pH conditions (i.e., 7.4 vs. 5.5) was measured by inductively coupled plasma mass spectrometry (ICP-MS), showing a rapid release of copper from Cu-COF at pH 5.5 and reaching its releasing plateau ≈72 h (Figure S5, Supporting Information). In contrast, the release of copper in pH 7.4 buffer solution was slower. The stable presence of Cu$^+$ was next verified. As a good Fenton-like reagent, Cu$^+$ could catalyze hydrogen peroxide (H_2O_2) overexpression in cells to produce ·OH and $^1O_2$, leading to cell death. However, Cu$^+$ was easily oxidized to Cu^{2+} in solution, losing the function of Fenton-like reagent. A selective sequestering agent Neocuproine (Neo) was applied to detect Cu$^+$ in Cu-COF. Once mixed with Cu$^+$, Neo would yield a yellow-colored chromophore,[18] which was ascribed to the formation of [Cu(neocuproine)$_2$]$^+$. Meanwhile, the characteristic absorption peak of the mixed solution at 450 nm increased significantly, which could be used to judge the existence of Cu$^+$. Therefore, we mixed COF and Cu-COF with Neo separately. To avoid the effect of the material on absorbance, the supernatant was centrifuged to observe and measure the ultraviolet-visible (UV-vis)
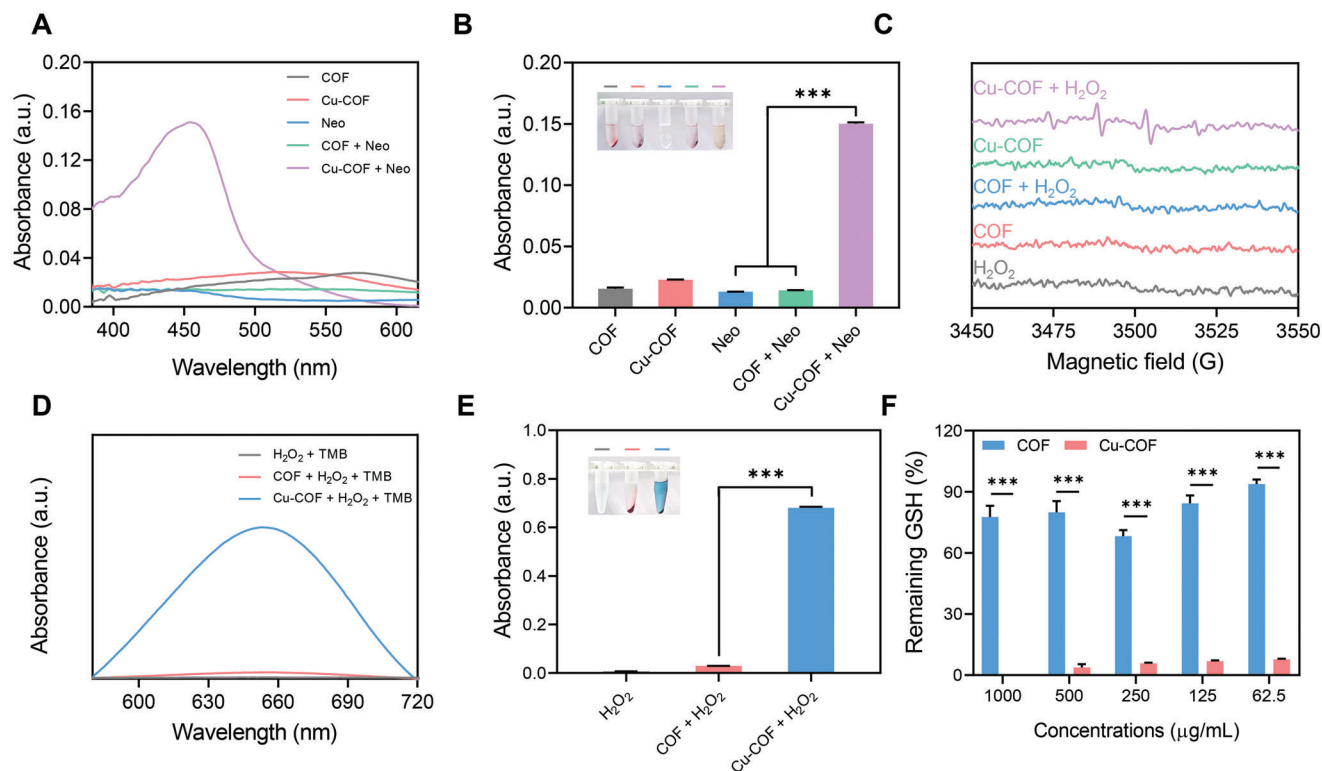
Figure 2. Functional characterization of Cu-COF. A,B) The ultraviolet-visible (UV-vis) absorption spectra and the absorbance at 450 nm of the supernatant of COF, Cu-COF, Neo, COF + Neo, and Cu-COF + Neo. Inset: the photographs of different solutions. C) The ESR spectra of H_2O_2, COF, and Cu-COF with or without H_2O_2 (100 μM) using DMPO as the trapping agent. D,E) The UV-vis absorption spectra and the absorbance at 650 nm of the supernatant of TMB incubated with H_2O_2, COF + H_2O_2, and Cu-COF + H_2O_2. Inset: the photographs of different solutions. (F) GSH elimination in vitro induced by Cu-COF. Data are presented as the mean ± SD ($n = 3$). Significant differences were assessed using a t-test (*$p < 0.05$, **$p < 0.01$, ***$p < 0.001$).

absorption spectrum. The results showed that the supernatants of COF, Cu-COF, Neo, and COF + Neo solutions were colorless and the absorption at 450 nm in the UV-vis absorption spectra was weak (**Figure 2**A,B and S5, Supporting Information). In contrast, Cu-COF produced a visible yellow color in the supernatant of the solution after mixing with Neo. The UV-vis absorption spectrum also showed significantly higher absorbance. These results showed that there was stable Cu^+ in Cu-COF, which might be due to the coordination effect helping to stabilize the existence of Cu^+ and making it not easy to be oxidized, which was consistent with the results of the XPS spectrum.

Subsequently, we verified the Fenton-like function of Cu^+ in Cu-COF. The H_2O_2-treated COF and Cu-COF were characterized using an Electron Paramagnetic Resonance (ESR) Spectrometer,[19] as shown in Figure 2C, using DMPO as the trapping agent. The H_2O_2 solution was first examined and no radical signal was found to be generated. In contrast, no free radical signal was evident for COF with or without the addition of H_2O_2, indicating that COF itself could not be used as a Fenton-like agent. For Cu-COF, there was also no free radical signal originally, but after the addition of H_2O_2, it showed the characteristic signal peak of DMPO/·OH adduct with the signal intensity of 1:2:2:1, which confirmed that Cu-COF and H_2O_2 could produce ·OH by Fenton-like reaction, indicating that Cu-COF was an excellent Fenton-like agent.

TMB turns blue when encountering ·OH, so it was often used to detect whether materials could generate ·OH through Fenton or Fenton-like effect.[20] Figure 2D showed the UV-vis absorption spectra of the supernatants of COF and Cu-COF mixed with H_2O_2. The photograph of the solution and the absorbance at 650 nm was shown in Figure 2E. It could be seen that H_2O_2 and COF alone could not produce blue color with TMB, indicating that no ·OH was produced. When Cu-COF was mixed with H_2O_2, there was a clear blue color production, indicating the production of ·OH in the Cu-COF + H_2O_2 solution. Combined with the fact that the Cu-COF solution in Figure 2A was also colorless, it showed that the Cu-COF solution could produce ·OH only in the presence of H_2O_2, indicating the ability of Cu-COF to produce the Fenton-like effect, which provided encouragement for subsequent cell killing.

Considering that both TMB and Cu-COF are positively charged, we introduced the negative 2, 2'-Azinobis-(3-ethylbenzthiazoline-6-sulphonate) (ABTS) to further verify whether the charge will affect the ROS generation ability of Cu-COF. Cu^{2+} can catalyze H_2O_2 and ABTS and change the absorbance of the solution. Therefore, we measured the UV-Visible absorption spectrum of Cu-COF and ABTS solution, and the results were as shown in Figure S7, Supporting Information. When there was only COF or only ABTS, the solution absorption was very weak after adding H_2O_2. However, when COF and

ABTS were mixed with H_2O_2, the 418 nm characteristic absorption was obvious. Color changes were visible to the naked eye. It shows that Cu-COF has good catalytic ability even in negative charge reagent.

The role of Cu^{2+} was next verified. Endogenous intracellular glutathione (GSH) could inhibit copper toxicity by acting as a sulfhydryl-containing copper chelate. The presence of Cu^{2+} eliminated intracellular GSH, thereby increasing the amount of ROS produced by Fenton-like effect and increasing its killing effect on cells. The concentration of intracellular GSH was simulated using a GSH standard. After incubation with the material, the remaining GSH content was detected using a GSH assay kit. The results were shown in Figure 2F, where there was only a trace change in GSH after COF treatment, indicating that COF had almost no effect on GSH elimination. In contrast, even the lowest concentration of 62.5 µg mL^{-1} Cu-COF treatment resulted in <10% of the original GSH content. At the same concentration, the ability of Cu-COF to consume GSH was much greater than that of COF, indicating that the presence of Cu^{2+} in Cu-COF was able to carry out GSH consumption effectively, which provided support for subsequent intracellular GSH depletion and killing of tumor cells.

At this point, we had completed the verification of the functionality of mixed-valence copper within Cu-COF. The results in Figure 2 showed that after the completion of coordination with COF, part of Cu^{2+} underwent a valence shift and was found to be stably loaded in Cu-COF as verified by the Neo reagent. On the one hand, the generated Cu^+ became an effective Fenton-like reagent, and in the presence of H_2O_2, Cu^+ catalyzed the production of ·OH from H_2O_2, which produced a signal in the ESR spectrum and gave a visible blue color with the TMB. On the other hand, the remaining Cu^{2+} could effectively deplete GSH and enhance the killing effect of Fenton-like effect on tumors. Mixed-valence copper in Cu-COF jointly enhanced the production and killing potency of ·OH.

2.3. Cellular Characterization of Cu-COF In Vitro

Encouraged by the previous functional validation, we verified whether Cu-COF could still have a good double-enhanced Fenton-like effect intracellularly. CT26 cells were selected to validate the endocytosis results and the combined treatment effect of Cu-COF.

Firstly, we labeled Cu-COF with Cy5 fluorescence, and the intracellular Cy5 fluorescence signal intensity was detected by flow cytometry after incubation with CT26 cells at different times. As shown in **Figure 3**A,B, flow cytometry assays were performed for both Control and Cu-COF groups incubated for 2 h, 4 h, and 6 h, respectively, and the resulting mean fluorescence intensity (MFI) values were compared. The results showed that the fluorescence intensity of intracellular Cu-COF increased with the increase of incubation time. The increase was obvious from 2 h to 4 h and only weakly increased between 4 h and 6 h. It indicated that Cu-COF could be well endocytosed into the cells and most of the endocytosis of Cu-COF was largely completed at ≈4 h. We then observed the cellular endocytosis of Cu-COF by confocal laser scanning microscopy (CLSM), and the results were displayed in Figure 3C and Figure S8, Supporting Information. Comparison with DAPI-stained nuclei and bright fields showed that Cy5-labeled Cu-COF was endocytosed into the cytoplasm to function with a high endocytosis efficiency.

We subsequently verified that Cu-COF exerts Fenton-like reagent after being endocytosed by the cells (Figure 3D,E). The DCFH-DA probe could be hydrolyzed by intracellular esterase upon entry into cells to generate non-fluorescent DCFH, which could be oxidized by intracellular ROS to fluorescent DCF. Therefore, the detection of DCF fluorescence could determine the level of intracellular reactive oxygen species. CT26 cells treated by the different methods were incubated with the DCFH-DA probe and then observed using a fluorescence microscopy. As shown in Figure 3D, no fluorescence was generated in both the Control and COF-treated group, while there was a large amount of green fluorescence in the Cu-COF-treated group, indicating a large amount of ROS generation in the Cu-COF-treated group, which was consistent with the previous validation results and illustrated that the stable loaded of Cu^+ in Cu-COF could act as a good Fenton-like reagent to generate intracellular ROS. SOSG was used as a probe to detect intracellular $^1O_2$ production.[14b] The largest amount of green fluorescence produced by Cu-COF indicated a large amount of $^1O_2$ production, while almost no fluorescence was produced in the Control and COF-treated group.

The ability of Cu-COF on intracellular GSH depletion was also verified. As shown in **Figure 4**A, compared with the Control group, COF caused almost no effect on intracellular GSH content, and increasing the concentration of COF also caused almost no change. In contrast, the GSH content started to decrease after Cu-COF treatment, and GSH in vitro decreased more significantly with increasing concentrations of Cu-COF. It showed that Cu-COF could significantly cause the depletion of intracellular GSH compared to COF.

High intracellular ROS production caused LPO. We examined the levels of malondialdehyde (MDA) within the different treatment groups. The results in Figure 4B showed that compared to the Control group, there was almost no change in the COF-treated group, while the level of MDA in the Cu-COF-treated group rose to be twofold, implying that Cu-COF induced a large amount of LPO.

Next, we verified the damaging effect of Cu-COF generated on DNA. The plasmid DNA obtained in a standard plasmid extraction experiment should be in both nicked and supercoiled conformations. DNA molecules with the same sequence but different conformations migrate through the gel pores at different rates, so the damage to DNA could be determined by agarose gel electrophoresis experiments.[21] The results of Gel electrophoresis analysis of the reaction solutions after coincubation with different concentrations of COF and Cu-COF and H_2O_2 and pEGFP plasmids showed in Figure 4C. The DNA group alone had only two bands, indicating the structural integrity of the plasmid. After treatment with H_2O_2 and Cu-COF respectively, the structure of the plasmid was not affected and only two bands still existed. In contrast, the DNA in the COF-treated group remained without significant structural changes in the presence of H_2O_2, while the bands in the supercoiled form disappeared and the bands in both nicked and Linear forms increased in the Cu-COF-treated group in a concentration-dependent manner, indicating that ROS generated by Cu-COF-catalyzed H_2O_2 caused significant damage to DNA. At the maximum concentration of 100 µg mL^{-1}, no longer
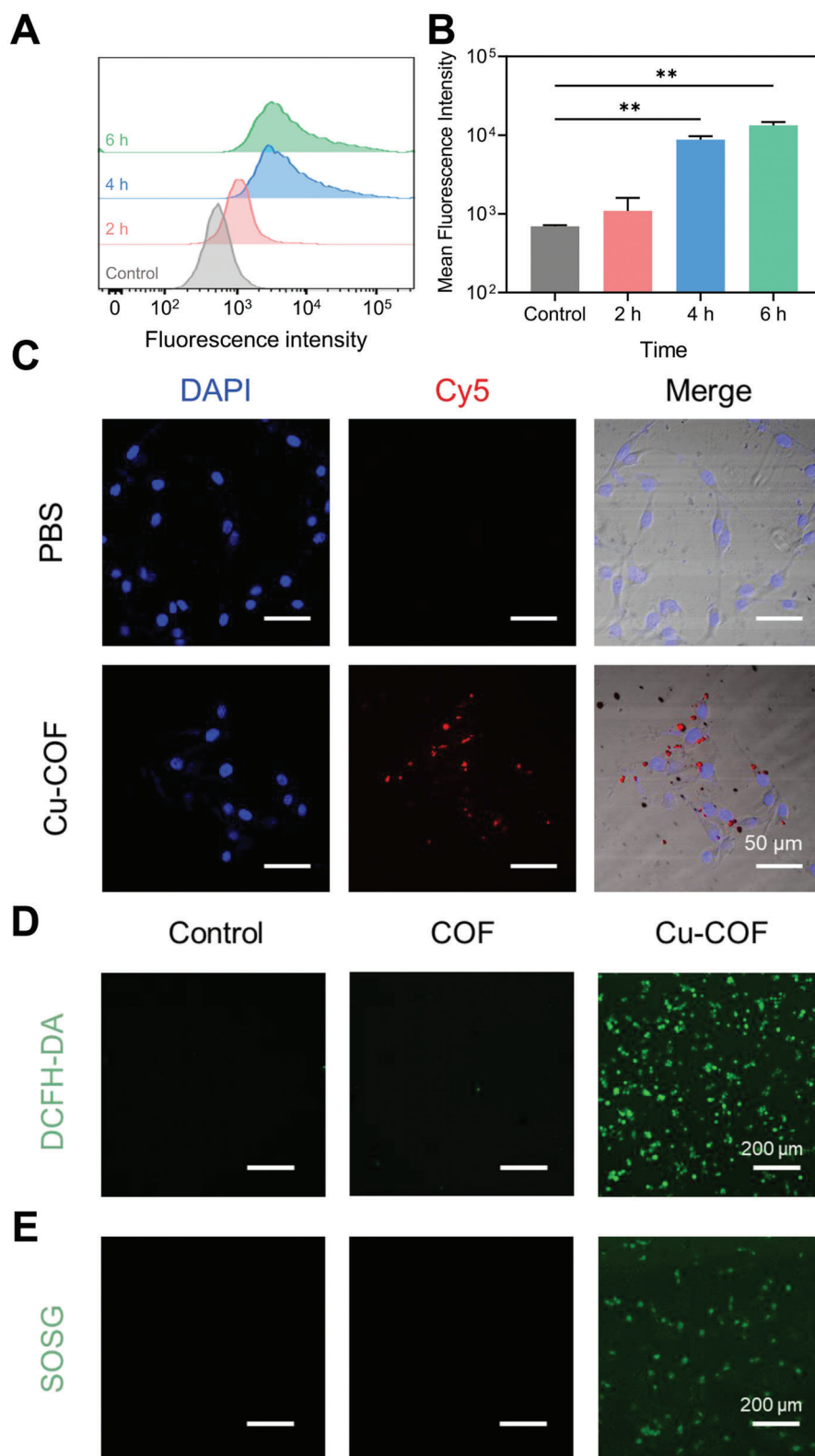
Figure 3. Cellular uptake and detection of intracellular ROS and $^1O_2$. A,B) Flow cytometry results of CT26 cells incubated with Cy5-Cu-COF for different times and the mean fluorescence intensity of each group. C) CLSM images of CT26 cells treated with Cy5-Cu-COF for 6 h, scale bar = 50 μm. D) Detection of ROS. Fluorescence microscopy images of DCFH-DA stained CT26 cells after incubated with COF and Cu-COF, scale bar = 200 μm. E) Detection of $^1O_2$. Fluorescence microscopy images of SOSG stained CT26 cells after incubated with COF and Cu-COF, scale bar = 200 μm. Data are presented as the mean ± SD ($n = 3$). Significant differences were assessed using a t-test (*$p < 0.05$, **$p < 0.01$, ***$p < 0.001$).

**ADVANCED
SCIENCE NEWS**

www.advancedsciencenews.com

[M] **acro-
olecular
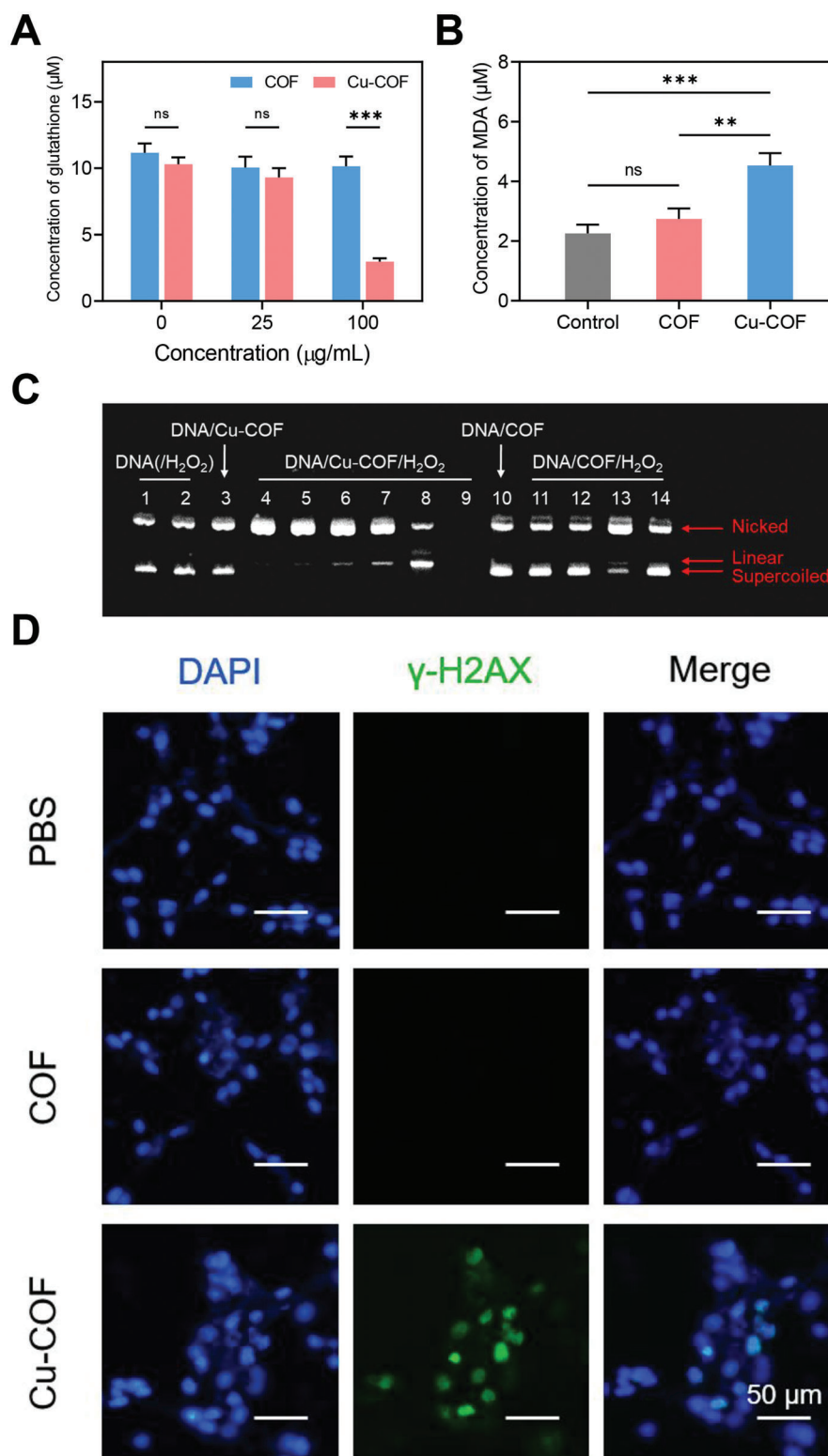Rapid Communications**

www.mrc-journal.de

Figure 4. Study of the effect of COF on CT26 cells. A) Cu-COF-induced GSH elimination in vitro. B) Cu-COF-induced lipid peroxidation (LPO) in vitro. Data are presented as the mean $\pm$ SD ($n = 3$). Significant differences were assessed using a t-test (*$p < 0.05$, **$p < 0.01$, ***$p < 0.001$). C) ROS-evoked DNA damage. **1**: DNA. **2**: DNA/H_2O_2. **3**: DNA/Cu-COF. **4–9**: DNA/Cu-COF/H_2O_2 (Concentration of Cu-COF (μg mL^{-1}): 3.125, 6.25, 12.5, 25, 50, 100). **10**: DNA/COF. **11–14**: DNA/COF/H_2O_2 (Concentration of COF (μg mL^{-1}): 12.5, 25, 50, 100). D) γ-H2AX immunofluorescence staining, scale bar = 50 μm.
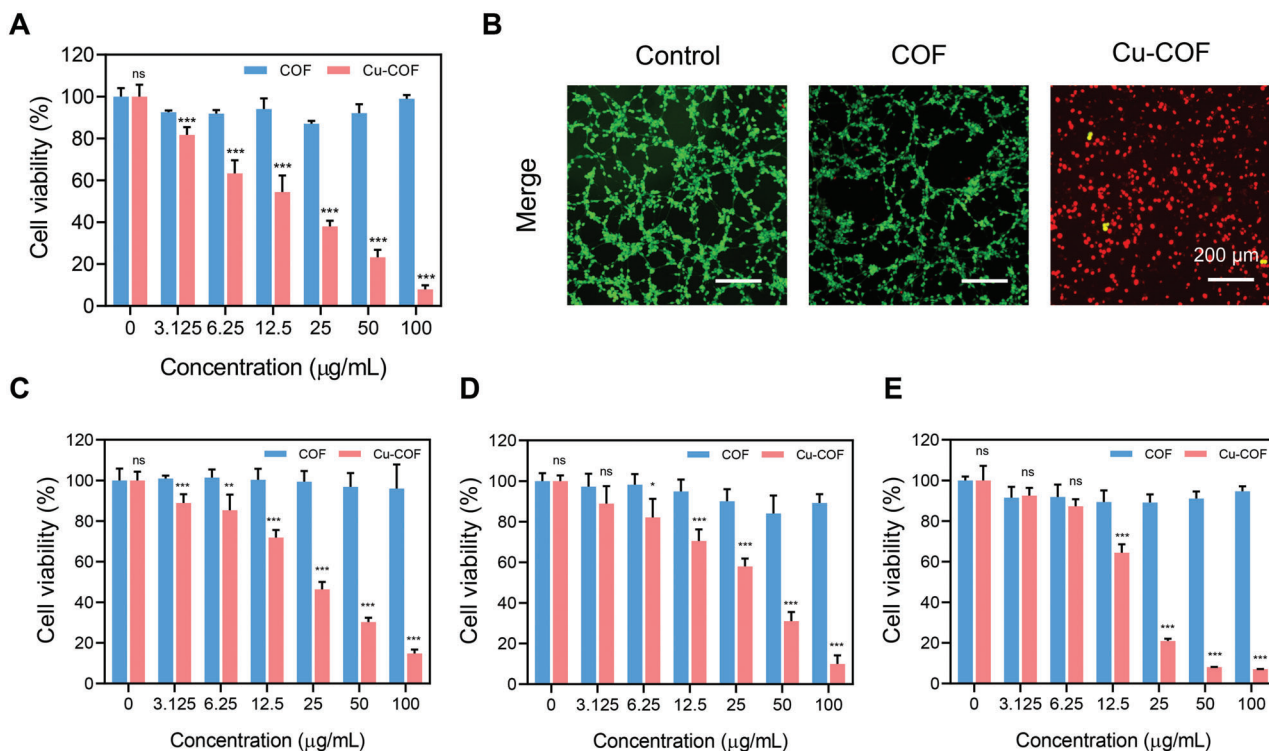
Figure 5. Cytotoxicity of Cu-COF. A) The relative viabilities of CT26 cells after incubation with different concentrations of COF and Cu-COF. B) Fluorescence microscopy images of calcein-AM and propidium iodide costained CT26 cells after incubation with COF and Cu-COF, scale bar = 200 μm. C–E) The relative viabilities of 4T1 cells, B16F10 cells, and HeLa cells after incubation with different concentrations of COF and Cu-COF. Data are presented as the mean ± SD ($n = 3$). Significant differences were assessed using a t-test ($*p < 0.05$, $**p < 0.01$, $***p < 0.001$).

visible bands were evident. After increasing the exposure intensity (Figure S9, Supporting Information), many smaller DNA bands were found, we inferred that too much ROS made the DNA break into small fragments and therefore migrate at a greater rate in gel electrophoresis.

Immunofluorescence staining with the DNA double-strand break marker γ-H2AX was used to detect intracellular Cu-COF-induced DNA damage.[22] As shown in Figure 4D, after Cu-COF treatment, there was a clear fluorescence colocalization of DAPI and γ-H2AX in the nucleus, indicating strong DNA damage caused by the dual ROS generated in the cells.

2.4. Validation of Cytotoxicity and Triggering of ICD

The performance of Cu-COF in vitro encouraged us to explore the cytotoxicity of Cu-COF. CT26 cells were still selected for validation. As in **Figure 5**A, cell viability was measured by Cell Counting Kit-8 (CCK-8) after material treatment. The results showed that COF had almost no effect on cell viability, which remained >90% even at the maximum concentration of 100 μg mL^{-1}, indicating the good biocompatibility of COF. In contrast, after the coordination of copper, Cu-COF produced significant cytotoxicity and showed concentration dependence. Cell survival decreased with increasing Cu-COF concentrations. At a concentration of 100 μg mL^{-1}, cell viability was already below 10%, indicating that Cu-COF could cause significant cytotoxicity to CT26 cells (IC50: 23.88 μg mL^{-1}). The cells were then stained for Live & Dead with

Calcein-AM and PI, respectively. The results in Figure 5B and Figure S10, Supporting Information, were consistent with those of CCK-8.

To verify the general cytotoxicity of Cu-COF, we also performed CCK-8 experiments on other common murine-derived tumor cells, including 4T1 cells, B16F10 cells, and HeLa cells, using COF as a control, and the results were displayed in Figure 5C–E. The results were similar to those in CT26 cells, demonstrating the good biocompatibility of COF and the excellent anti-tumor properties after Cu coordination. Similarly, we calculated the IC50 values of Cu-COF to different cells, as shown in Figure S11. The results were similar to those in CT26 cells, demonstrating the good biocompatibility of COF and the excellent anti-tumor properties after Cu coordination.

ICD is an effective means of enhancing CD8$^+$ T cell infiltration. It increases the immune response of T cells by releasing tumor-associated antigens and damage-associated molecular patterns, which in turn triggers effective antigen presentation. An important trigger of ICD is intracellular ROS. After completing the validation of the intracellular properties and cytotoxicity of Cu-COF, we verified the induction of ICD by Cu-COF. Calmodulin (CRT) exposure and release of HMGB1 is an important feature of ICD. We labeled Cu-COF-treated cells with anti-CRT antibodies and examined them by flow cytometry, and the results were shown in **Figure 6**A, the MFIs were calculated in Figure 6B. The fluorescence intensity of COF-treated cells was essentially the same as that of the control group, while the CRT content on the cell surface was significantly increased after Cu-COF treat-
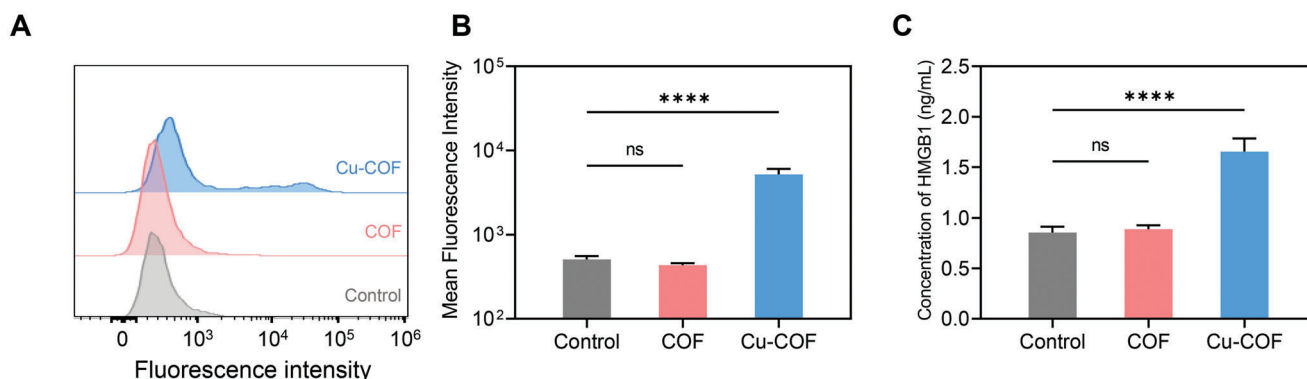
Figure 6. Validation of immunogenic cell death. A,B) Flow cytometry results of CT26 cells stained with anti-CRT antibody after incubated with COF and Cu-COF and the mean fluorescence intensity of each group. C) Detection of extracellular HMGB1 by ELISA kit. Data are presented as the mean ± SD (n = 3). Significant differences were assessed using a t-test (*$p < 0.05$, **$p < 0.01$, ***$p < 0.001$).

ment. Meanwhile, Figure 6C showed that the secretion of cellular HMGB1 was significantly increased after Cu-COF treatment. These results suggested that Cu-COF could induce immune death of tumor cells with the potential of immunotherapy and enhanced CD8$^+$ T cell infiltration.

3. Conclusion

In conclusion, we successfully prepared Fenton-like regent Cu-COF by performing the coordination of Cu based on the COF-TpAzo. In the process of coordination, the valence transfer of Cu^{2+} occurred, resulting in Cu^{2+} and Cu$^+$ loaded simultaneously in the final prepared Cu-COF, which was proved by the XPS results. Upon entering the cell, Cu$^+$ catalyzed the decomposition of overexpressed hydrogen peroxide (H$_2$O$_2$) in the cell, producing ·OH and ^{1}O$_2$, causing significant DNA damage and LPO, which could directly kill the tumor cells. Meanwhile, Cu^{2+} consumed GSH to convert it into glutathione disulfide (GSSG), which reduced the ability to scavenge ROS, thus further enhancing the Fenton-like effect and intensifying intracellular oxidative stress, bringing stronger toxic effects to CT26 cells. At a concentration of 100 µg mL^{-1}, cell viability was already below 10%. These two therapeutic modalities eventually worked synergistically to induce robust ICD, reflected in the obvious calreticulin (CRT) exposure and release of HMGB1, which had the potential to increase the infiltration of CD8$^+$ T cells, converting "cold tumor" to "hot tumor" as well as more powerful anti-tumor effects. We also verified the toxicity of Cu-COF to other types of tumor cells, and the results showed that this strategy could also significantly inhibit the growth of tumor cells such as 4T1, B16F10, and HeLa, indicating the universality of the Cu-COF. The coordinated COF synthesized in this paper was an effective strategy to modulate the TME, which was a meaningful exploration of the application of COF in immunotherapy, and was expected to inspire more designs for the application of COF in tumor therapy.

4. Experimental Section

Preparation of COF and Cu-COF: The synthesis of COF was carried out by referring to the previous reports. Azo monomer (9.5 mg) and Tp monomer (6.5 mg) were dissolved with dichloromethane (250 mL) respec-

tively, and trifluoroacetic acid (10 uL) was added to the dichloromethane solution of Azo at room temperature, followed by the dichloromethane solution of Tp and stirred at room temperature for three days. Most of the dichloromethane was removed by rotary evaporation, and petroleum ether was added for sedimentation. The COF was collected by centrifugation, followed by washing with N, N-dimethylacetamide, acetone, and deionized water, and then dried using a vacuum oven. The Cu-COF was then prepared as follows. COF (10 mg) and anhydrous copper sulfate (CuSO$_4$, 167 mg) were weighed, added N, N-dimethylformamide (5 mL), condensed and refluxed at 120 °C for 24 h, then collected by centrifugation, washed with water to remove the unreacted anhydrous copper sulfate, and dried using a vacuum oven. The Cu-COF was obtained as a purple powder.

Detection of Cu$^+$ in Cu-COF by Neocuproine: Neocuproine was dissolved with ethanol and then diluted 5 times with deionized water to prepare a 1 mM Neo solution. After mixed 375 µL of PB buffer solution (pH = 6.2), 400 µL of Neo solution, and 500 µL of Cu-COF aqueous solution (1 µg mL^{-1}), the UV-visible absorption spectrum was detected after mixing well. The other materials were treated similarly and measured. The absorbance at 450 nm was recorded.

Detection of ·OH Generation: DMPO was used as a probe to capture ·OH. The electron spin resonance spectra were detected using Electron Paramagnetic Resonance Spectrometer after mixing aqueous Cu-COF solution with aqueous H$_2$O$_2$ solution (100 µM) and adding 4 µL of DMPO solution (10 mM). Meanwhile, TMB was used as a probe to detect ·OH. UV-visible absorption spectra were performed after incubation of TMB with aqueous Cu-COF solution (1 mg mL^{-1}), and absorbance at 650 nm was recorded.

Cell Culture: CT26 cells and B16F10 cells were cultured using Roswell Park Memorial Institute (RPMI) 1640 medium, and 4T1 cells and HeLa cells were cultured using Dulbecco's Modified Eagle Medium (DMEM) medium, which contains 10% Fetal bovine serum (FBS) and 1% antipenicillin streptomycin. All cells were cultured in an incubator (37 °C, 5% CO$_2$).

Cellular Uptake: CT26 cells were inoculated in 24-well plates with 1 × 10^5 cells per well, and continued to be cultured in the cell culture incubator for 24 h. After the cells were plastered, Cy5-labeled Cu-COF was added to the wells and incubated for different times, the supernatant was discarded, the cells were washed with PBS twice and collected after trypsin digestion, washed twice with PBS by centrifugation to remove the free Cu-COF and dispersed in PBS. The fluorescence intensity of the cells was detected by flow cytometry (Thermo ATTUNE NXT).

CT26 cells were inoculated in a 6-well plate containing coverslips with 1.5 × 10^5 cells per well and continued to be cultured in a cell culture incubator for 24 h. After the cells were plastered, Cy5-labeled Cu-COF was added to the wells, and after incubation for different times, the supernatant was discarded, and the cells were washed twice with PBS and incubated with 4% paraformaldehyde for 15 min to fix the cells, washed 5 times with PBS, and then stained with The cells were washed 5 times with PBS, stained with

**ADVANCED
SCIENCE NEWS**

www.advancedsciencenews.com

[M] acro-
molecular
Rapid Communications

www.mrc-journal.de

DAPI for 5 min, washed 5 times with PBS, the coverslips were removed, fixed on slides, sealed with glycerol, photographed and observed using a confocal fluorescence microscope (Zeiss LSM980).

Evaluation of Intracellular ROS Generation: CT26 cells were inoculated in 24-well plates with 6×10^4 cells per well, and continued to be cultured in the cell culture incubator for 24 h. After the cells were plastered, COF and Cu-COF were added to the wells respectively and continued to incubate for another 6 h. After the supernatant was discarded, a DCFH-DA probe diluted 1000 times with a serum-free medium was added. After incubation at 37 °C for 20 min, the wells were washed three times with serum-free medium and observed by fluorescence microscopy.

Cytotoxicity: CT26 cells were inoculated in 96-well plates with 8×10^3 cells per well, and continued to be cultured in the cell culture incubator for 24 h. After the cells were plastered, COF and Cu-COF were added to the wells respectively and continued to incubate for another 24 h. The supernatant was discarded, and 100 µL of the medium was added to each well, followed by 10 µL of CCK-8 solution. After continuing incubation in the incubator for 2 h, the absorbance of each well at 450 nm was measured using an enzyme marker (Thermo Scientific Varioskan LUX). 4T1 cells, B16F10 cells, and HeLa cells were also treated with the same method. Cell viability was calculated as follows:

$$\text{Cell viability (\%)} = A_T / A_C \times 100\% \tag{1}$$

A_T is the absorbance of the material treatment group and A_C is the absorbance of the Control group.

Validation of ICD: CT26 cells were inoculated in 24-well plates with 1×10^5 cells per well, and continued to be cultured in the cell culture incubator for 24 h. After the cells were plastered, COF and Cu-COF were added to the wells respectively and continued to incubate for another 12 h. The supernatant was discarded and the cells were washed twice with PBS, collected by trypsin digestion, washed twice by centrifugation with PBS, stained with the anti-CRT-FITC antibody at 4 °C, further washed twice with PBS, and finally dispersed in PBS, and the fluorescence intensity of the cells was detected by flow cytometry.

CT26 cells were inoculated in 96-well plates with 8×10^3 cells per well and continued to be cultured in the cell culture incubator for 24 h. After the cells were plastered, COF and Cu-COF were added to the wells respectively and continued to incubate for another 24 h. The supernatant was collected and tested according to the instructions of the HMGB1 assay kit.

Statistical Analysis: Data analysis was performed using Microsoft Excel and GraphPad Prism 8 software. The data were presented as mean ± s.d. All of the statistical analysis was compared by Student's t-test (*$p < 0.05$ was considered statistically significant. **$p < 0.01$ and ***$p < 0.001$ were considered extremely significant).

Supporting Information

Supporting Information is available from the Wiley Online Library or from the author.

Conflict of Interest

The authors declare no conflict of interest.

Data Availability Statement

Research data are not shared.

[1] Y. Wang, Y. Ding, D. Yao, H. Dong, C. Ji, J. Wu, Y. Hu, A. Yuan, *Small* **2021**, *17*, 2006231.

[2] L. Voorwerk, M. Slagter, H. M. Horlings, K. Sikorska, K. K. Van De Vijver, M. De Maaker, I. Nederlof, R. J. C. Kluin, S. Warren, S. Ong, T. G. Wiersma, N. S. Russell, F. Lalezari, P. C. Schouten, N. A. M. Bakker, S. L. C. Ketelaars, D. Peters, C. A. H. Lange, E. Van Werkhoven, H. Van Tinteren, I. A. M. Mandjes, I. Kemper, S. Onderwater, M. Chalabi, S. Wilgenhof, J. B. A. G. Haanen, R. Salgado, K. E. De Visser, G. S. Sonke, L. F. A. Wessels, et al., *Nat. Med.* **2019**, *25*, 920.

[3] Y.-T. Liu, Z.-J. Sun, *Theranostics* **2021**, *11*, 5365.

[4] a) H. Liang, X. Wu, G. Zhao, K. Feng, K. Ni, X. Sun, *J. Am. Chem. Soc.* **2021**, *143*, 15812; b) I. Mellman, G. Coukos, G. Dranoff, *Nature* **2011**, *480*, 480.

[5] a) D. V. Krysko, A. D. Garg, A. Kaczmarek, O. Krysko, P. Agostinis, P. Vandenabeele, *Nat. Rev. Cancer* **2012**, *12*, 860; b) Y. Song, Y. Sun, M. Tang, Z. Yue, J. Ni, J. Zhao, W. Wang, T. Sun, L. Shi, L. Wang, *ACS Appl. Mater. Interfaces* **2022**, *14*, 4914; c) M. Tang, Z. Zhang, C. Ding, J. Li, Y. Shi, T. Sun, C. Chen, *J. Colloid Interface Sci.* **2022**, *627*, 299.

[6] a) Y. Li, P. Zhao, T. Gong, H. Wang, X. Jiang, H. Cheng, Y. Liu, Y. Wu, W. Bu, *Angew. Chem., Int. Ed.* **2020**, *59*, 22537; b) A. P. Cote, A. I. Benin, N. W. Ockwig, M. O'keeffe, A. J. Matzger, O. M. Yaghi, *Science* **2005**, *310*, 1166; c) J. Zhou, W. Zhao, Z. Miao, J. Wang, Y. Ma, H. Wu, T. Sun, H. Qian, Z. Zha, *ACS Nano* **2020**, *14*, 2126; d) M. Tang, Y. Shi, L. Lu, J. Li, Z. Zhang, J. Ni, W. Wang, Y. Zhang, T. Sun, Z. Wu, *Chem. Eng. J.* **2022**, *449*, 137847.

[7] a) Y. Tian, R. Tian, L. Chen, R. Jin, Y. Feng, Y. Bai, X. Chen, *Macromol. Rapid Commun.* **2019**, *40*, 1800824; b) T. Nie, W. Zou, Z. Meng, L. Wang, T. Ying, X. Cai, J. Wu, Y. Zheng, B. Hu, *Adv. Mater.* **2022**, *34*, 2206286.

[8] Y. Yu, Z. Huang, Q. Chen, Z. Zhang, H. Jiang, R. Gu, Y. Ding, Y. Hu, *Biomaterials* **2022**, *288*, 121724.

[9] S. Sheng, F. Liu, M. Meng, C. Xu, H. Tian, X. Chen, *CCS Chem.* **2022**, *4*, 2321.

[10] a) B. Ma, S. Wang, F. Liu, S. Zhang, J. Duan, Z. Li, Y. Kong, Y. Sang, H. Liu, W. Bu, L. Li, *J. Am. Chem. Soc.* **2019**, *141*, 849; b) Y. Yang, J. Tang, P. L. Abbaraju, M. Jambhrunkar, H. Song, M. Zhang, C. Lei, J. Fu, Z. Gu, Y. Liu, C. Yu, *Angew. Chem., Int. Ed.* **2018**, *57*, 11764; c) F. Wang, T. Qiu, Y. Ling, Y. Yang, Y. Zhou, *Angew. Chem., Int. Ed.* **2022**, *61*, e202209499.

[11] P. Tsvetkov, S. Coy, B. Petrova, M. Dreishpoon, A. Verma, M. Abdusamad, J. Rossen, L. Joesch-Cohen, R. Humeidi, R. D. Spangler, J. K. Eaton, E. Frenkel, M. Kocak, S. M. Corsello, S. Lutsenko, N. Kanarek, S. Santagata, T. R. Golub, *Science* **2022**, *375*, 1254.

[12] Y. Xu, S.-Y. Liu, L. Zeng, H. Ma, Y. Zhang, H. Yang, Y. Liu, S. Fang, J. Zhao, Y. Xu, C. R. Ashby, Y. He, Z. Dai, Y. Pan, *Adv. Mater.* **2022**, *34*, 2204733.

[13] N. K. Pandey, L. Chudal, J. Phan, L. Lin, O. Johnson, M. Xing, J. P Liu, H. Li, X. Huang, Y. Shu, W. Chen, *J. Mater. Chem. B* **2019**, *7*, 6630.

[14] a) G. Zhang, X. Li, Q. Liao, Y. Liu, K. Xi, W. Huang, X. Jia, *Nat. Commun.* **2018**, *9*, 2785; b) Q. Guan, L.-L. Zhou, Y.-A. Li, W.-Y. Li, S. Wang, C. Song, Y.-B. Dong, *ACS Nano* **2019**, *13*, 13304; c) S. Gan, X. Tong, Y. Zhang, J. Wu, Y. Hu, A. Yuan, *Adv. Funct. Mater.* **2019**, *29*, 1902757;

d) S. Yao, M. Zheng, S. Wang, T. Huang, Z. Wang, Y. Zhao, W. Yuan, Z. Li, Z. L. Wang, L. Li, *Adv. Funct. Mater.* **2022**, *32*, 2209142.

[15] F. Liu, S. Sheng, D. Shao, Y. Xiao, Y. Zhong, J. Zhou, C. H. Quek, Y. Wang, J. Dawulieti, C. Yang, H. Tian, X. Chen, K. W. Leong, *Matter* **2021**, *4*, 3677.

[16] H. S. Sasmal, A. Halder, S. Kunjattu H, K. Dey, A. Nadol, T. G. Ajithkumar, P. Ravindra Bedadur, R. Banerjee, *J. Am. Chem. Soc.* **2019**, *141*, 20371.

[17] Y. Shi, S. Liu, Y. Liu, C. Sun, M. Chang, X. Zhao, C. Hu, M. Pang, *ACS Appl. Mater. Interfaces* **2019**, *11*, 12321.

[18] W. Feng, Liu, Z., Xia, L., Chen, M., Dai, X., Huang, H., Dong, C., He, Y., Chen, Y., *Angew. Chem., Int. Ed.* **2022**, *61*, e202212021.

[19] J. M. Lázaro-Martínez, L. V. Lombardo Lupano, L. L. Piehl, E. Rodríguez-Castellón, V. Campo Dall' Orto, *J. Phys. Chem. C* **2016**, *120*, 29332.

[20] D. Wang, L. Lin, T. Li, M. Meng, K. Hao, Z. Guo, J. Chen, H. Tian, X. Chen, *Adv. Mater.* **2022**, *34*, 2205924.

[21] Y. Li, Z. Li, Hu Hou, Y. Zhuang, L. Sun, *Molecules* **2018**, *23*, 2263.

[22] A. Kinner, W. Wu, C. Staudt, G. Iliakis, *Nucleic Acids Res* **2008**, *36*, 5678.